Electronic Supplementary Information

Elucidating the Influence of Side Chains on the Self-Assembly of Semi-Flexible Mesogens

Table of contents

S1. Materials 3
S2. Thermal analysis of the star-shaped molecules 4
S3. Structure analysis of the Cr phase of molecule 1a-1 4
a. Density measurements of the Cr phase 5
b. Electron density profile 5
c. Description of the model of the Cr phase....6
d. Simulation of the diffraction pattern of molecule 1a-1 9
S4. Structural analysis of the family of star-shaped derivatives....10
S5. Morphological analysis of thin films of star-shaped derivatives....14
References....16

S1. Materials

A series of star-shaped mesogens based on the phloroglucinol core having different degrees of flexibility of the arms have been synthesized. The synthesis is described elsewhere.[1,2]

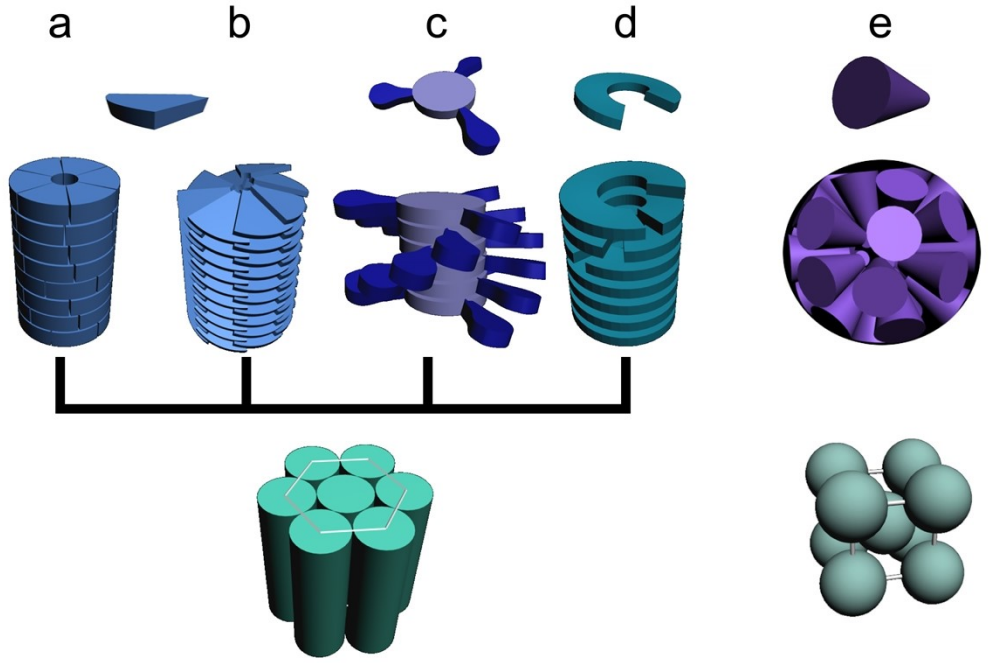

Figure S1. Various helical organizations of different molecules. **a, b**- Helical columns formed by wedge-shaped molecules, similar to those observed in monodendrons. **c-** Helices composed of discotic molecules with C3 symmetry bearing bulky arms. **d**- Helical columns formed by molecules capable of adopting a helical conformation. **e**- Spherical self-assemblies of conical monodendrons, organized into complex 3D super-structures.

S2. Thermal analysis of the star-shaped molecules

The phase transition temperatures and associated enthalpy changes have been measured with a Mettler Toledo 822e heat-flux Differential Scanning Calorimetry (DSC). The heating rate employed was 10 °C/min. The results are collected in Table S1.

Upon cooling from the isotropic phase (I) to room temperature (RT), mesogens **1a-1** through **1a-4** show the presence of a columnar hexagonal disordered mesophase (Col_{hd}). This phase is metastable in compound **1a-1** and transforms isothermally into a more ordered crystalline-like helical phase (Cr). A similar behavior is observed for molecules **1c-1** and **1d**, with the monotropic phase being absent only in mesogen **1b-1**, which has longer and consequently more flexible arms.

Table S1: Phase transitions of star-shaped mesogens measured by DSC

Compound	Phase transitions, $\xrightarrow{Tonset/T\max,\Delta HJ/g}$
1a-1	$Col_{hd} \xrightarrow{53.0/53.9,2} I$ $Cr^{*} \xrightarrow{55.4/60.3,12.7} I$
1a-2	$Col_{hd} \xrightarrow{50.7/52.0,1.3} I$
1a-3	$Col_{hd} \xrightarrow{50.3/52.1,4} I$
1a-4	$Col_{hd} \xrightarrow{70.9/73.2,1.6} I$
1b-1	$Cr \xrightarrow{78.0/83.5,4.0} Col_{hd} \xrightarrow{97.4/98.1,1.1} I$
1c-1	$Cr^{*} \xrightarrow{57.8/61.8,3.3} I$
1d-1	$Col_{hd} \xrightarrow{52.5/53.2,2.43} I$ $Cr^{*} \xrightarrow{49.3/55.0,9.4} I$

*measured after annealing for 15 hours at room temperature
Col_{hd}- columnar hexagonal disordered phase, Cr- crystalline-like helical phase, I- isotropic phase

S3. Structure analysis of the Cr phase of molecule 1a-1

The structure of the Cr phase formed by molecule **1a-1** was analyzed using X-ray diffraction on oriented fibers, which were prepared by extruding the material in its metastable Col_{hd} phase.

a. Density measurements of the Cr phase

The mass density of the **1a-1** fiber in the Cr phase was measured using the pycnometer method. The density (ρ) is calculated using the formula: $\rho = N*M_w / V_m*N_A$, where N represents the number of molecules per columnar slice, M_w is the molecular weight, V_m is the volume of the unit cell, and N_A is the Avogadro's number. The measured density was 1.01 g/cm^3. Based on the lattice parameters obtained from X-ray fiber diffraction patterns (a= 80.1 Å, b =36.9 Å), it can be determined that one columnar slice contains 24 molecules.

b. Electron density profile

The experimental X-ray diffraction pattern for **1a-1** shows up to ten diffraction orders of the fiber repeat peak, suggesting the presence of a superstructure along the columnar axis. The Z-

projection of the electron density profile (EDP) was calculated using Lorentz-corrected intensities of the meridional peaks, I_n, using the following approach:

$$E(z) = \sum_{n=0}^{N} A_n \cos(\frac{2\pi n\ z}{c} + \varphi_n)\ ,$$

where $A_n=(I_n)^{1/2}$ is the amplitude of the n^{th} diffraction order peak, *c* represents the periodicity in the z direction, and φ_n is the phase. The phase values (either 0 or π due to the centro-symmetric structure) were determined by comparing the EDP calculated from the experimental intensities of the meridional peaks for different phase sets with the EDP profile obtained from our structural models. Only the phases of the most intense peaks, such as 002 and 004, were varied, while the phases of the remaining peaks were fixed at zero.

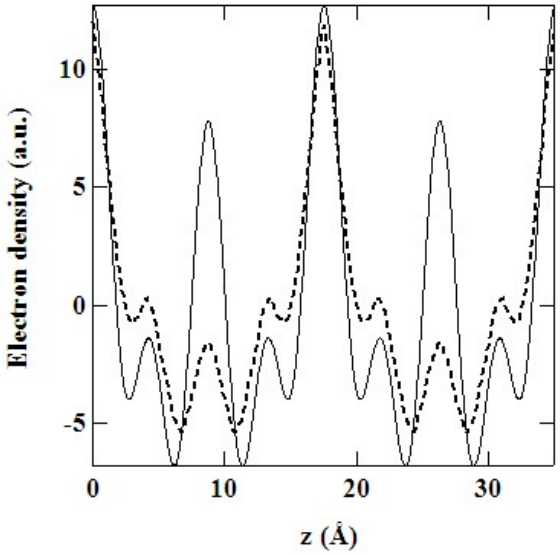

Figure S2. EDPs corresponding to the experimental (solid line) and model (dashed line) structures, respectively.

The best agreement was achieved when all phases were set to zero. Figure S2 presents the experimental meridional X-ray scattering profile alongside the corresponding EDP. The analysis revealed that the constitutive element in the columnar direction has a thickness of 17.5Å.

c. Description of the model of the Cr phase

Energy minimization for different conformations of the molecules and columns was performed using the Materials Studio package (BIOVIA), while X-ray diffraction patterns were simulated using custom modules compiled for XOP and integrated with IGOR PRO (Wavemetrics Ltd.).

Due to the flexibility of the molecular core, molecule **1a-1** can adopt a range of conformations. Simple rotations about the C-O bond do not alter the molecules' C3 symmetry; however, changes in the torsion angle significantly impact molecular shape. Two primary conformations were identified: the star-shaped and E-shaped conformers. The choice of the E-shaped conformer was determined based on the following considerations.

If the molecules were to adopt a star-shaped conformation, a large amount of unoccupied space would remain in the center of the column, which presents an issue. Additionally, to form a helical column, the molecules would need to rotate uniformly around the column axis, which would only generate a single fundamental peak in the meridional direction of the X-ray diffraction pattern – contradicting the experimental data. Therefore, it is more plausible that, in the double helix (Cr phase), the molecules adopt the E-shaped conformation.

The E-shaped conformation, with the middle phenyl oriented at 60 degrees out of the molecular plane, was refined using the *Discover* module in the Materials Studio package (BIOVIA). The calculated thickness of each element (about 17.5 Å) aligns with the maxima observed in the EDP, confirming of four structural elements per repeat unit. This implies that each structural element of the double helix is composed of three molecules. The relative positions of the neighboring elements within the lattice were refined by comparing simulated and experimental meridional intensities. Simulated intensities for various relative shifts (0, c/10, c/12, c/15, and c/24 in the z-direction) are shown in Figure S3.

The double helix is formed by rotating the hexamolecular aggregate, which contains two structural elements, by 90 degrees. The best match to the experimental intensity is obtained when the two constitutive elements are positioned at the same height, accurately reproducing the experimental observation that the 004 diffraction order is stronger than the 002, while the 006 is significantly weaker.

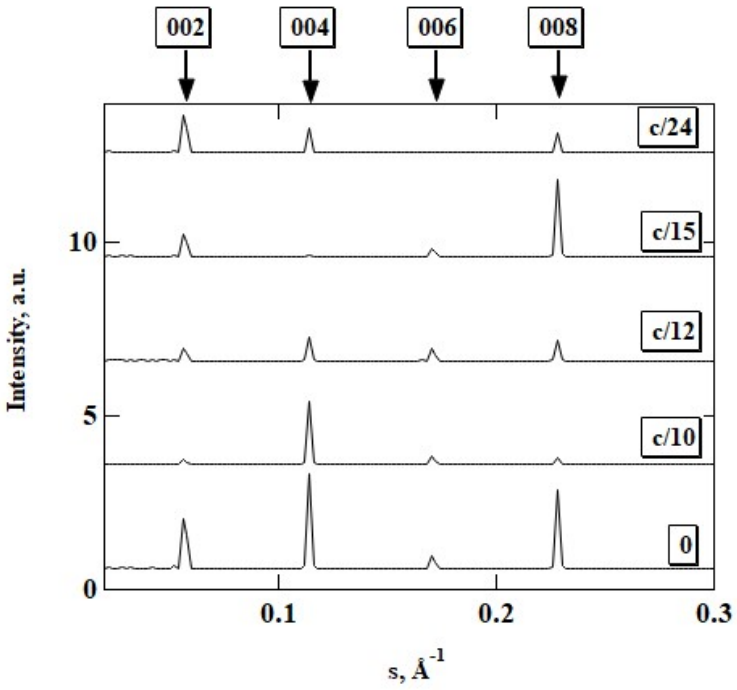

Figure S3. Simulated meridional intensity for the different relative shifts of the trimolecular building elements in one hexamolecular cluster.

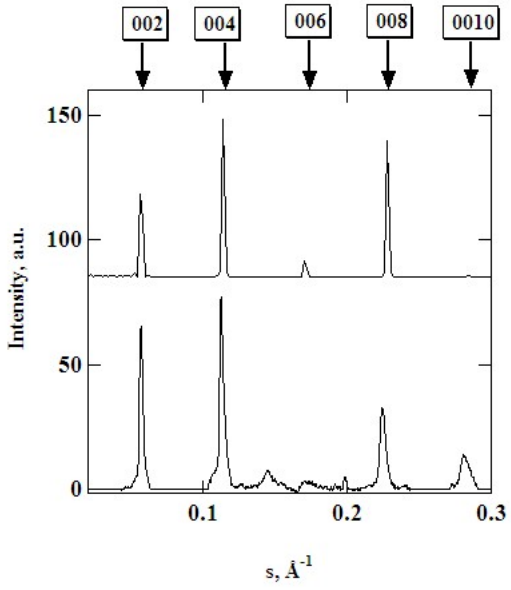

Figure S4. Comparison of the experimental scattered intensity along the meridian (bottom) and the simulated intensity calculated for zero relative shift of the trimolecular building elements in one hexamolecular cluster (top).

As evident from Figure S4, the simulated and experimentally measured scattered intensities for the proposed model show a good agreement. It is important to highlight that in all of the conducted simulations, the lateral chains were not considered. This omission underscores that

the primary structural features are well captured by the model, even without accounting for the lateral chain contributions.

It is important to note that shifting or rotating the structural elements within the (ab) plane does not affect the diffraction pattern in the meridional direction. To further refine our structural model, we compared simulated AFM images with the experimental ones. The simulated AFM images were generated using a custom-built routine that calculated the topography "visible" to an AFM tip of a finite size. Figures S5 and S6 present two examples of molecular models for the structural elements, along with the corresponding AFM simulations. The closest match to the experimentally obtained high-resolution AFM image was observed in the simulated double helices, where no lateral shift or rotation between the structural elements was present (Fig. 3c,d).

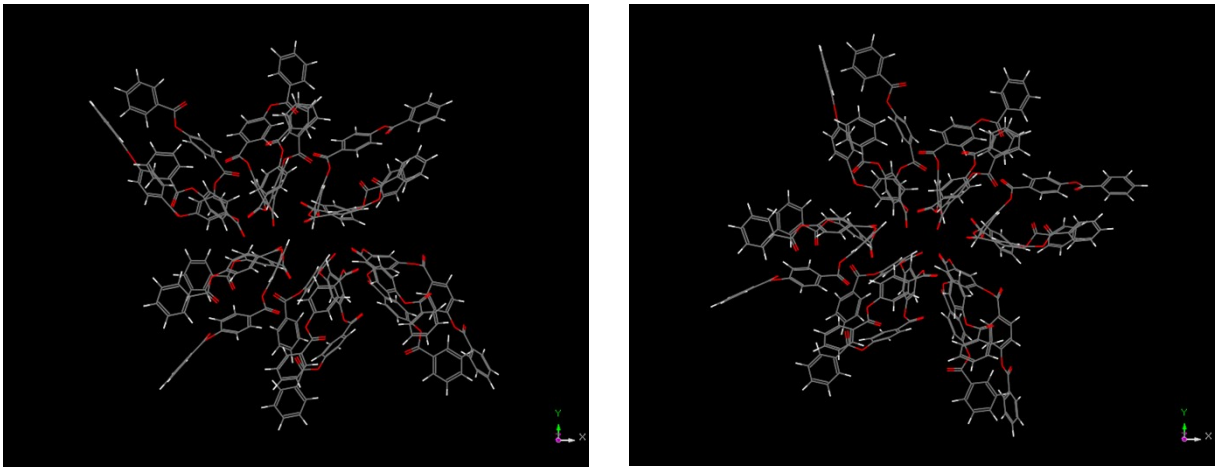

Figure S5. Molecular models of the structural elements of the double helix laterally shifted by 5Å (left) and rotated about the vertical axis by 20º (right).

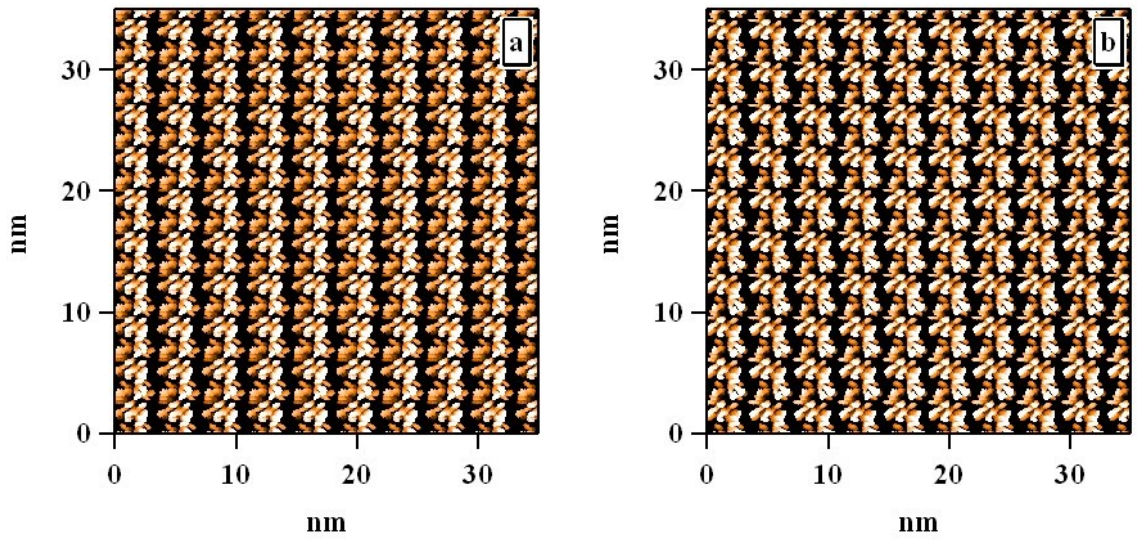

Figure S6. Simulated AFM images computed for the double helices with the elements shifted by 5 Å within the (ab) plane (**a**) and rotated about the vertical axis by 20º (**b**).

d. Simulation of the diffraction pattern of molecule 1a-1

For the optimization of the columnar positions in the (ab) plane, the 2D fiber diffraction calculation of the supramolecular structure of **1a-1** was performed using a custom-built procedure in IGOR PRO software (Wavemetrics Ltd.). The alkyl chains were excluded from the calculation. The scattering intensity I(s) in reciprocal space was calculated according to the following equation:

$$(\rightarrow)\left|\sum \rightarrow\right|$$

where f_i and r_i represent the atomic scattering factor and coordinates for each atom in the unit cell, respectively. The Fourier transform was calculated using a triangular window function. The scattered intensity I(s) was then transformed into a 2D diffraction pattern according to the following formula:

$$I(s_r, s_z) = I(\sqrt{s_x^2 + s_y^2}, s_z)$$

where s_r and s_z are horizontal and vertical projections of the reciprocal space s-vector. Before performing the calculations, geometry optimization of the unit cell was carried out using the Forcite module in the Materials Studio package (BIOVIA). The pattern in Figure S7 was calculated for a crystal with dimensions 5a x 5b x 5c, where a, b, and c represent the unit cell parameters. The step sizes for the calculations were set to 0.001 Å for s_r (equatorial direction) and 0.002 Å for s_z (columnar direction). This fine grid allows for accurate reproduction of the diffraction features corresponding to the crystallographic structure of the sample.

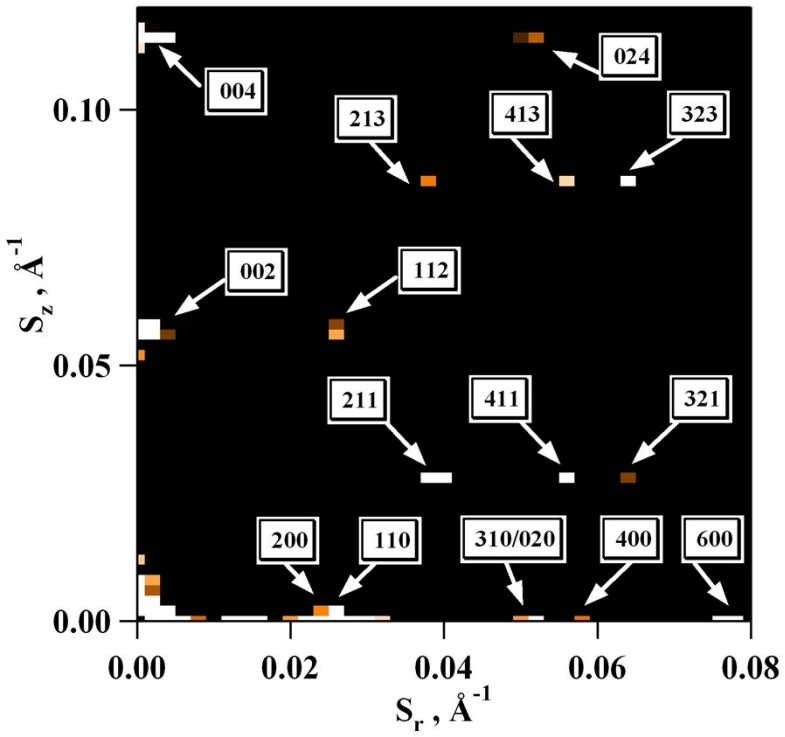

Figure S7. Simulated 2D X-ray diffraction pattern corresponding to the Cr phase of mesogen **1a-1**.

S4. Structural analysis of the family of star-shaped derivatives

X-ray diffraction measurements were carried out on oriented fibers, and the results are summarized in Table S2. The corresponding X-ray diffraction patterns for molecules 1b-1, 1c, and 1d are displayed in Figures S8, S9, and S10, respectively. These patterns provide insights into the molecular packing and crystalline structures of the star-shaped derivatives, revealing key differences in the arrangement of molecules based on their arm length and core flexibility. The detailed analysis of these diffraction patterns provides insights for understanding the relationship between molecular structure and phase behavior.

Table S2. Temperature dependent X-ray diffraction data on oriented samples

Compound	Phase	hkl	d_{exp} [Å]	d_{calc} [Å]	Lattice parameters [Å]	Density [g/cm^3]
1a-1	Col_{rd} (RT)	100 200	37.98 18.60 4.7 (halo)	37.98 18.5	a=42.7	0.99 (measured)

	Cr (RT*)	200 110 310 400 120 600 620 211 002 112 413 233 004 10 2 4 005 235 007 008 0 0 10	40.13 33.50 21.60 20.10 18.04 13.35 10.91 21.32 17.59 15.74 9.69 8.36 8.83 5.59 6.90 6.12 4.98 4.40 3.51	40.10 33.52 21.65 20.05 17.98 13.37 10.82 21.50 17.61 15.58 9.77 8.31 8.81 5.64 7.04 6.04 5.03 4.40 3.52	*a*=80.2 *b*=36.9 c=35.2	1.2 (measured)
1a-2	Col_{hd} (RT)	100 200 4.5 (halo)	36.00 18.24	36.00 18.00	a=41.57	
1a-3	Col_{hd} (RT)	100 200 4.4 (halo)	36.93 18.75	36.93 18.46	a=42.64	
1a-4	Col_{hd} (RT)	100 200 4.4 (halo)	37.61 19.14	37.61 18.81	a=43.43	
1b-1	Cr (RT)	010 110 1-10 210 2-10 020 120 2-20 201 211 002	42.52 36.10 34.72 25.91 25.25 21.88 21.10 16.78 21.55 19.57 15.75	43.73 36.67 34.81 25.92 24.61 21.87 20.98 17.40 21.85 19.86 15.45	*a*=61.9 *b*=43.8 *c*=30.9 γ=86.9	
	Col_{hd} (110°C)	100 110 200	43.75 25.18 21.85 4.8 (halo)	43.75 25.26 21.87	*a*=50.52	
1c	Col_{hd} (RT)	100 110 200	37.2 21.52 18.73 4.4 (halo)	37.2 21.48 18.6	*a*=42.95	

	Cr (RT*)	100 110 200 002 004 006 241 110	35.8 21.1 18.3 15.92 8.29 5.43 10.53 4.33 4.4 (halo)	35.8 20.66 17.9 15.92 7.96 5.30 10.49	a=41.3 b= c=31.84	

1d	Cr (RT)	200 020 400 420 4-20 040 620 060 640/060 800 460 840 660 8-40 080 680 4 10 0/10 8 0 12 8 0/2 12 0 6 12 0/16 0 0 10 12 0/0 14 0 111 301 311 521 741 002 202 222 042 622 062 662 113 223 253 743 763 004 404 044 125 355 006 426 6 12 8 529 4 0 10 1 1 11 0 0 12 0 0 14 0 0 15	38.22 31.44 19.12 17.43 16.62 15.8 12.12 10.74 10.28 10.09 9.15 8.65 8.32 7.92 7.53 6.67 5.96 5.19 4.91 4.32 39.22 24.48 21.37 13.99 9.29 31.75 24.28 18.99 13.95 11.29 10.16 8.03 19.12 15.32 10.34 8.42 7.00 15.75 12.25 11.10 11.43 8.37 9.95 8.72 4.10 6.31 5.93 5.54 5.71 4.42 3.84	39.05 31.21 19.52 16.96 16.17 15.60 12.24 10.40 10.26/10. 40 9.76 9.39 8.48 8.34 8.09 7.80 6.85 6.04/5.67 5.13/5.19 4.91/4.88 4.44/4.46 39.01 24.02 22.79 13.91 9.21 31.15 24.35 19.51 13.95 11.39 9.87 8.06 19.18 15.98 10.44 8.49 7.31 15.76 12.18 11.02 11.48 8.45 10.38 8.85 4.16 6.23 5.94 5.62 5.19 4.45 3.79	*a*=78.2 *b*=62.5 *c*=62.3 γ=87	

		0 0 17 0 0 18 0 6 18	3.75 3.45 3.38	3.66 3.46 3.28		
	Col_{hd} (RT)	100	38.5 4.8 (halo)		*a*=44.5	

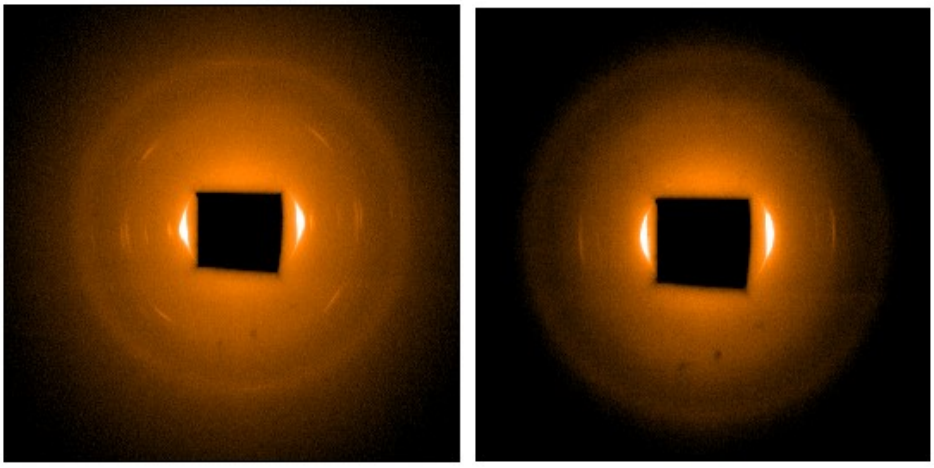

Figure S8. X-ray diffraction pattern of mesogens **1b-1** at ambient temperature (left) and at 110 °C (right).

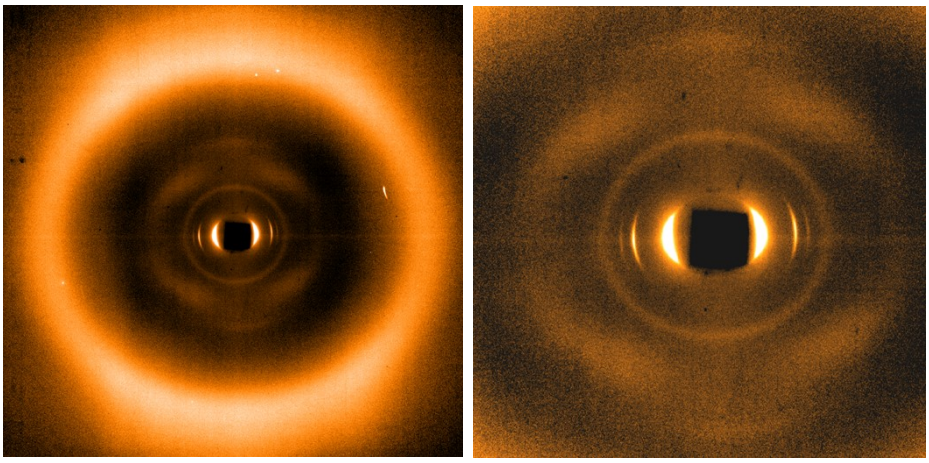

Figure S9. X-ray diffraction pattern of mesogen **1c-1** at ambient temperature (left) with a close-up view of the small-angle region.

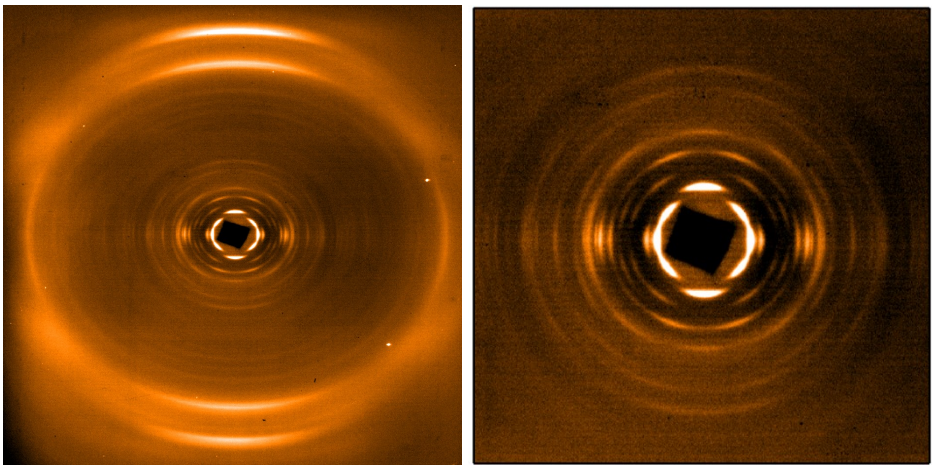

Figure S10. X-ray diffraction pattern of the sample of **1d-1** annealed at ambient temperature (left) with a close-up view of the small-angle region (right).

Figure S11 shows the constitutive structural element of a double helix formed by mesogen **1c-1**.

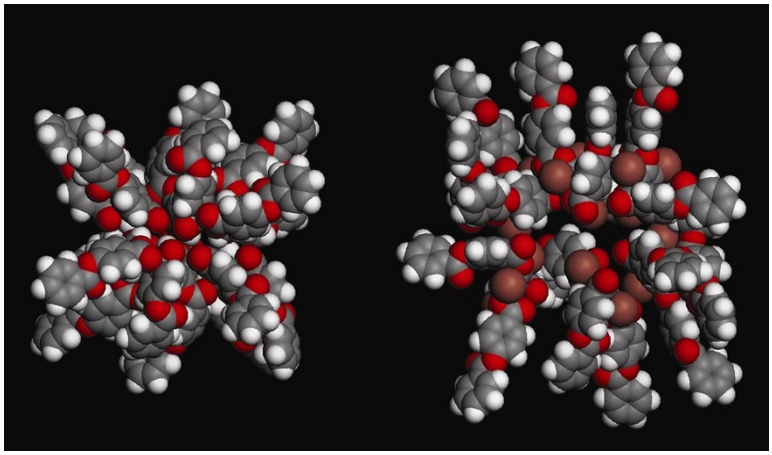

Figure S11. Comparison of the constitutive elements of the double helices formed by mesogens **1a-1** (left) and **1c-1** (right).

S5. Morphological analysis of thin films of star-shaped derivatives

The surface morphology of thin spin-coated films was investigated using an atomic force microscope (Bruker Nanoscope III) in Tapping mode. Time-resolved AFM measurements were performed by repeatedly imaging the same region of the sample. High-resolution images of the columnar morphology were obtained using Hi'Res probes (Mikromasch) with ultrasharp whiskers grown at the AFM tip.

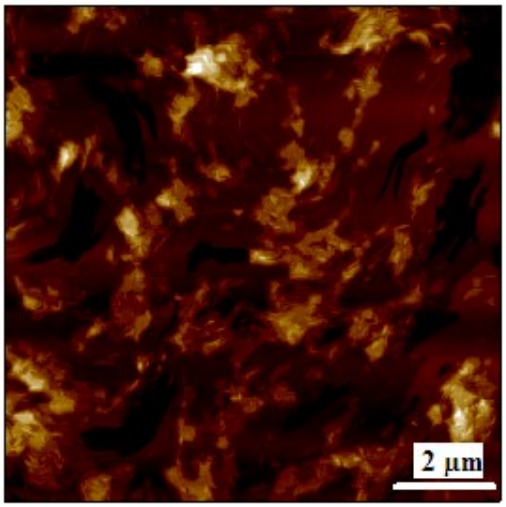

Figure S12. Large-scale AFM topography image of a spin-coated film formed by mesogen **1b-1**.

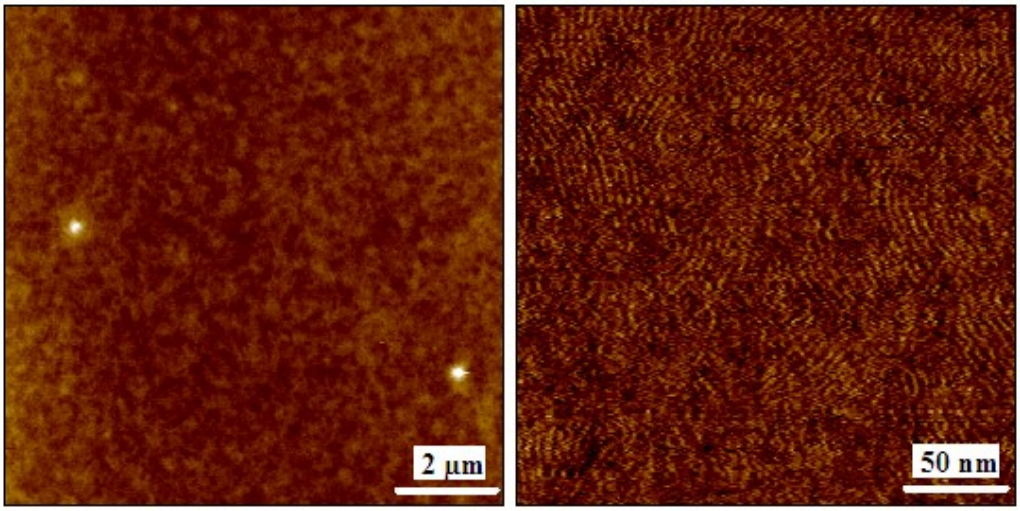

Figure S13. AFM topography images of a spin-coated film formed by mesogen **1c-1**, captured at large (left) and small scale (right).

References

1. M. Lehmann, R.I. Gearba, M. H. J. Koch, D. A. Ivanov, *Mol. Cryst. & Liq. Cryst.,* 2004, **411**, 397–406.
2. M. Lehmann, R.I. Gearba, M. H. J. Koch, D. A. Ivanov, *Chem. Mater.,* 2004, **16**, 374–376.